J Membrane Biol (2007) 215:81–92
DOI 10.1007/s00232-007-9008-1

Temperature Dependence of Steady-State and Presteady-State Kinetics of a Type IIb Na^+/P_i Cotransporter

Andrea Bacconi · Silvia Ravera · Leila V. Virkki · Heini Murer · Ian C. Forster

Received: 11 October 2006 / Accepted: 6 January 2007 / Published online: 19 April 2007

Abstract The temperature dependence of the transport kinetics of flounder Na^+-coupled inorganic phosphate (P_i) cotransporters (NaPi-IIb) expressed in *Xenopus* oocytes was investigated using radiotracer and electrophysiological assays. $^{32}P_i$ uptake was strongly temperature-dependent and decreased by ~80% at a temperature change from 25°C to 5°C. The corresponding activation energy (E_a) was ~14 kcal mol^{-1} for the cotransport mode. The temperature dependence of the cotransport and leak modes was determined from electrogenic responses to 1 mM P_i and phosphonoformic acid (PFA), respectively, under voltage clamp. The magnitude of the P_i- and PFA-induced changes in holding current decreased with temperature. E_a at –100 m*V* for the cotransport and leak modes was ~16 kcal mol^{-1} and ~11 kcal mol^{-1}, respectively, which suggested that the leak is mediated by a carrier, rather than a channel, mechanism. Moreover, E_a for cotransport was voltage-independent, suggesting that a major conformational change in the transport cycle is electroneutral. To identify partial reactions that confer temperature dependence, we acquired presteady-state currents at different temperatures with 0 mM P_i over a range of external Na^+. The relaxation time constants increased, and the peak time constant shifted toward more positive potentials with decreasing temperature. Likewise, there was a depolarizing shift of the charge distribution, whereas the total available charge and apparent valency predicted from single Boltzmann fits were temperature-independent. These effects were explained by an increased temperature sensitivity of the Na^+-debinding rate compared with the other voltage-dependent rate constants.

Keywords P_i cotransport · Uncoupled leak · Temperature · Presteady-state · Activation energy

A. Bacconi · S. Ravera · L. V. Virkki · H. Murer · I. C. Forster (✉)
Institute of Physiology and Center for Integrative Human Physiology, University of Zurich, Winterthurerstrasse 190 CH-8057 Zurich, Switzerland
e-mail: IForster@access.unizh.ch

Introduction

Secondary active transporters are solute carrier proteins that mediate the uphill movement of a specific solute by coupling this to the downhill movement of a specific ion (e.g., H^+, K^+ or Na^+) according to the free energy available from the driving ion's own electrochemical gradient. The coupling confers a strict stoichiometric ratio between the driven and driving species. This contrasts with the traditional view of ion channels, which, when in the conducting or open state, allow solute movement through their pore according to an electrodiffusive mechanism, thereby resulting in transport rates up to five orders of magnitude faster than for carriers. The kinetic and molecular models proposed to account for the functional data also reflect these differences between carriers and channels, and the activation energy for movement of an ion through a channel is much less than that associated with the transport cycle of a carrier (Van Winkle 1995). This underscores a thermodynamically based distinction between channels and carriers that is reflected in the greater apparent complexity of the conformational changes involved in the translocation process in the latter case, where ordered substrate binding/debinding and alternating accessibility of substrates to their respective binding sites are features of the currently postulated carrier mechanisms. Recently, the distinction between carriers and channels has become less clear as

evidenced by a number of studies on cotransporters that have identified leak modes in the absence of substrate and which exhibit channel-like properties (DeFelice 2004; Sonders and Amara 1996). Moreover, studies on the serotonin transporter (SERT) indicate that at high substrate concentrations SERT exhibits transport behavior more consistent with a channel rather than a carrier (Adams and DeFelice 2002). Finally, functional studies on a bacterial homolog of the ClC channel have revealed that a single-amino acid substitution can switch the mode of operation from that of an H^+:Cl^- antiporter with strict stoichiometric coupling to the characteristic ClC channel mode (Accardi and Miller 2004).

Electrogenic type II Na^+-coupled inorganic phosphate (P_i) cotransporters (NaPi-II), encoded by members of the solute carrier *SLC34* gene family (http://www.biopara-digms.org), also possess the expected strict stoichiometrically coupled cotransport mode behavior of a carrier (Forster, Loo and Eskandari 1999; Virkki et al. 2005b) as well as leak-mode behavior (Forster et al. 2002). A Na^+-dependent leak mode for the rat NaPi-IIa cotransporter was proposed from the finding that the P_i transport inhibitor phosphonoformic acid (foscarnet or PFA), applied in the absence of P_i to NaPi-IIa-expressing *Xenopus* oocytes under voltage-clamp conditions, led to a decrease in the holding current (Forster et al. 1998). The magnitude of the PFA-induced change in holding current was proportional to the cotransport mode activity, which suggested a direct association of this pathway with functional expression of the cotransporter. Moreover, its reversal potential was reported to shift in a Nernstian manner according to the external Na^+ concentration (Forster et al. 1998). The NaPi-IIa Na^+-leak mode was incorporated into a kinetic scheme as a ''uniporter'' pathway (Forster et al. 1998), similar to that proposed for other Na^+-driven cotransporters (e.g., the sodium glucose cotransporter [SGLT1] [Birnir, Loo and Wright 1991; Chen et al. 1997], the thyroid Na^+/I^- cotransporter [Eskandari et al. 1997] and the Na^+-dependent dicarboxylate cotransporter [Yao and Pajor 2000]). This scheme indicates that the leak and cotransport modes are mutually exclusive but share the same empty carrier and Na^+ binding transitions. Studies involving both wild-type and mutant NaPi-IIa constructs (Kohler et al. 2002a, b; Virkki et al. 2005b) have also provided experimental evidence in support of this idea. Nevertheless, the reversal potential of I_{PFA} lies far to the left (typically –20 m*V* with external 100 mM Na^+) of what would be predicted if Na^+ were the only ion involved, and this observation therefore suggests that I_{PFA} is more complex than originally proposed. Moreover, recent observations (A. Bacconi, L. V. Virkki and I. C. Forster, unpublished results) indicate that Cl^- ions may also be involved, which adds further weight to the concept, proposed for excitatory amino acid cotransporters, that a transporter-associated, substrate-gated, channel-like pathway could also be present (e.g., Otis and Jahr 1998).

The distinction between carrier and leak modes can be experimentally demonstrated by determining their temperature dependence, based on the property that the activation energy for translocating solutes according to a carrier mechanism is significantly greater than that associated with ionic electrodiffusion for a channel (Van Winkle 1995). This hypothesis is supported by studies on a serotonin transporter (dSERT) (Beckman and Quick 2001) and a γ–aminobutyric acid (GABA) transporter isoform (GAT4) (Karakossian et al. 2005), in which significantly different temperature coefficients for the respective cotransport and leak modes were reported.

The aims of the present study were twofold. First, to gain further insight into the mechanism of the NaPi-II cotransport and leak modes, we determined the temperature dependence of the respective transport rates. We used the type IIb Na^+/P_i cotransporter (NaPi-IIb) cloned from flounder because of its 5- to 10-fold higher expression in *Xenopus* oocytes (Forster et al. 1997) compared with its mammalian cousins. We have previously shown that flounder NaPi-IIb exhibits leak and cotransport modes (Forster, Biber and Murer 2000) and displays similar kinetic features associated with the mammalian NaPi-IIa (Forster et al. 1997, 1999, 2000; Virkki, Murer and Forster 2006a, b). Therefore, our findings should be applicable to mammalian members of the SLC34 family. Second, to identify the contributions of resolvable partial reactions that comprise the overall cotransport cycle, we characterized the temperature dependence of presteady-state relaxations under different external superfusion conditions. Analysis of presteady-state relaxations allowed us to compare the temperature dependence of voltage-dependent partial reactions that precede P_i binding.

Materials and Methods

Reagents and Solutions

All reagents were obtained from Sigma (Buchs, Switzerland) or Fluka (Buchs, Switzerland).

The compositions of the solutions used (in mM) were as follows: oocyte incubation (modified Barth's solution), NaCl (88), KCl (1), $CaCl_2$ (0.41), $MgSO_4$ (0.82), $NaHCO_3$ (2.5), $Ca(NO_3)_2$(0.33) and 4-(2-hydroxyethyl)-1-piperazineethanesulfonic acid (HEPES, 7.5), adjusted to pH 7.6 with tris(hydroxymethyl)aminomethane (TRIS) and supplemented with antibiotics (10 mg/liter gentamycin or streptomycin or 5 mg/liter doxycyclin); control superfusate (ND100), NaCl (100), KCl (2), $CaCl_2$ (1.8), $MgCl_2$ (1) and

HEPES (10), adjusted to pH 7.4 with TRIS at room temperature; control superfusate (ND0), as for ND100 but with *N*-methyl-D-glucamine or choline chloride used to replace Na^+ (intermediate Na^+ concentrations were achieved by proportionate mixing of the ND100 and ND0 solutions); substrate test solutions, P_i added to ND100 from 1 M K_2HPO_4 and KH_2PO_4 stocks that were mixed to give pH 7.4.

For a change in temperature from 25°C to 2°C, the superfusate solution pH increased by 0.25 pH units, due to the $\log_{10}$ of acid dissociation constant (pKa) temperature dependence of the HEPES-TRIS buffer. Based on previous studies of the pH dependence of NaPi-IIa/b (Forster et al. 2000; Virkki et al. 2005a), this would result in a negligible change in electrogenic transport activity. Therefore, no pH adjustment was considered necessary in the present study.

Molecular Biology and Expression in *Xenopus laevis* Oocytes

The cDNA encoding for flounder NaPi-IIb was subcloned into a KSM expression vector to improve its expression in *X. laevis* oocytes, as described previously (Virkki et al. 2003). The plasmid was linearized using *Xba*1 (Promega, Madison, WI) and used as a template for the synthesis of capped cRNA using the Message Machine T3 kit (Ambion, Austin, TX). Stage V-VI defolliculated oocytes from *X. laevis* were isolated and maintained as described previously (Virkki et al. 2006b). Oocytes were injected with 50 nl of cRNA (0.2 μg/μl) encoding NaPi-IIb. Oocytes were incubated at 17°C in modified Barth's solution. Transport assays were performed 3–5 days after injection.

Tracer Uptake

The temperature dependence of P_i transport was determined by performing $^{32}P_i$ uptake assays at five different temperatures. Control oocytes and oocytes expressing NaPi-IIb (10–12 oocytes/group) were first allowed to equilibrate in ND100 solution without tracer at the appropriate temperature. After aspiration of this solution, we added 150 μl of ND100 solution containing 1 mM P_i and $^{32}P_i$ (specific activity 10 mCi/mmol P_i). After 30 min, the uptake was stopped by washing the oocytes four times with 3 ml ice-cold ND0 solution containing 0.5 mM cold P_i. Oocytes were then placed individually in scintillation vials and lysed in 250 μl 10% sodium dodecyl sulfate. $^{32}P_i$ activities of individual oocytes were measured using scintillation counting.

Electrophysiology

Electrophysiology was performed using a two-electrode voltage clamp (Geneclamp 500; Molecular Devices, Sunnyvale, CA). Oocytes were mounted in a small recording chamber (100 μl volume) and continuously superfused (~0.2 ml/min) with test solutions supplied using a peristaltic pump. The recording chamber was machined from a block of thermally conductive epoxy (ER2074; Electrolube, UK), which was mounted on a Peltier thermoelement (CP1.4–127–045L; Melcor, NJ). The chamber temperature was controlled by a laboratory-built electronic regulator. Data were acquired online using Digidata 1200 hardware and compatible pClamp8 software (Molecular Devices). Currents were prefiltered at a bandwidth less than twice the sampling rate appropriate for the signals being acquired. Steady-state and presteady-state currents were acquired using voltage steps from a holding potential V_h = –60 m*V* to test potentials in the range –180 to +80 m*V*. Presteady-state records were acquired with fourfold signal averaging. To account for the significant slowing of the presteady-state relaxations with temperature, the test pulse width was extended to ensure that the relaxations were complete before returning to the holding potential.

Data Analysis

Presteady Relaxations and Modeling

Relaxations induced by voltage steps were quantified by fitting a decaying double exponential function using a fitting algorithm (Clampfit, v. 8.0; Molecular Devices). To resolve the charge movement associated with the exogenous protein, a component subtraction method (Hazama, Loo and Wright 1997) was employed: the fast component, assumed to represent the oocyte capacitive charging, was extrapolated to the step onset and subtracted from the total transient current. The slower component was numerically integrated to give the charge attributable to the exogenous protein.

For a voltage step from a holding potential (V_h) to a test potential (V) that induces the movement of a charge Q, the Q-V data were fitted with a form of the Boltzmann equation:

$$Q = Q_{hyp} + Q_{max}/(1 + \exp(-ze(V - V_{0.5})/kT)) \quad (1)$$

The voltage dependence of the time constant (τ) of the slower relaxation induced by the voltage step was fitted as follows:

$$\tau = 1/(k_f \exp(-ze\,V/2kT) + k_b \exp(ze\,V/2kT)) \quad (2)$$

Eqs. 1 and 2 are derived from a simple Eyring transition rate model for a two-state system that describes the distribution and rate of movement of mobile charged particles (of effective valence, z) that move across the membrane over a symmetrical energy barrier, according to the direction and magnitude of the transmembrane electric field. For Eq. 1, Q_{max} is the maximum charge translocated, Q_{hyp} is

the steady-state charge at the hyperpolarizing limit and depends on V_h, $V_{0.5}$ is the voltage at which the charge is distributed equally between the two states, e is the elementary charge, k is Boltzmann's constant and T is the absolute temperature. For Eq. 2, k_f and k_b are the zero voltage forward and backward transition rates, respectively, for the relocation of the hypothetical particles according to a clockwise movement around the transport cycle. Based on this model, it can be shown that $V_{0.5} = -kT/ze \ln(k_b/k_f)$. Eqs.1 and 2 were fit to the Q-V and τ–V data, respectively, by nonlinear regression analysis with Q_{hyp}, Q_{max}, z, $V_{0.5}$, k_f and k_b as free parameters, for $T = 278$, 283, 288, 293 K. All curve fitting using Eqs. 1 and 2 was performed using the nonlinear regression analysis algorithms in GraphPad (San Diego, CA) Prism version 3.02/4.02 for Windows (http://www.graphpad.com).

Temperature Dependence

The Arrhenius equation (Segel 1976) was used for determining the temperature dependence of the transport kinetics:

$$k_r = A\exp(-E_a/RT) \tag{3a}$$

where k_r is the rate (uptake rate, substrate-induced current or partial reaction rate constant), A is a constant, R is the gas constant and E_a is the activation energy (in kcal mol^{-1}). Fitting with a single exponential function yields an estimate for E_a. Commonly, Eq. 3a can be recast in a logarithmic form and linear regression analysis applied to the experimental data to obtain E_a:

$$\log k_r = -E_a/(2.303R)(1/T) + \log A \tag{3b}$$

Both methods yield similar estimates for E_a, and we used the logarithmic graphical representation for consistency with other studies.

The temperature coefficient for a 10°C change, Q_{10}, is related to E_a as follows:

$$\log Q_{10} = 10E_a/(2.303RT1T2) \tag{4}$$

where T_1 and T_2 are the two temperatures (K).

Results

Temperature Dependence of Flounder NaPi-IIb in the Steady State

We first determined the temperature dependence of $^{32}P_i$ uptake for oocytes injected with flounder NaPi-IIb cRNA. Figure 1A shows that $^{32}P_i$ uptake exhibited a strong temperature dependence with an approximately fivefold increase with increasing temperature over the 20°C range used in these experiments. The uptake levels for noninjected oocytes were at least 50–100 times smaller than those for NaPI-IIb-expressing cells and showed no systematic temperature dependence. We therefore ignored the contribution of any endogenous uptake in the subsequent analysis. Figure 1B shows the same data for the NaPi-IIb-expressing oocytes replotted in the form of an Arrhenius plot (Segel 1976). The dependence of uptake rate (scaled logarithmically) on the reciprocal of absolute temperature

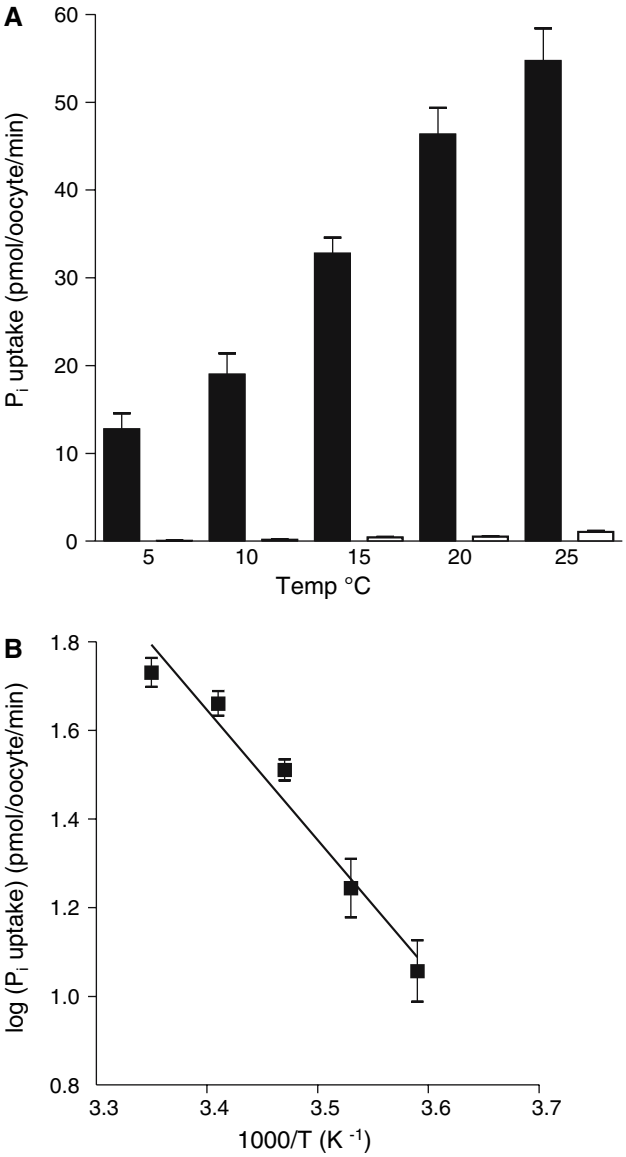

Fig. 1 Temperature dependence of $^{32}P_i$ uptake. (*A*) Uptake for NaPi-IIb-injected oocytes (*filled columns*) and noninjected oocytes (*empty columns*) from the same donor frog plotted as a function of incubation temperature. (*B*) Data for NaPi-IIb from *A* replotted as an Arrhenius plot (Eq. 3). The slope of the linear regression line was reported as –2,942 ± 335.3 K^{-1}, equivalent to E_a = 13.5 ± 1.5 kcal mol^{-1}

showed a reasonably linear relationship. We fit these data using a linear regression algorithm (r^2 = 0.96), and from the fitted slope we obtained an estimate of the apparent activation energy for the transport process, E_a = 13.5 ± 1.5 kcal mol^{-1}, which corresponds to a 10°C temperature coefficient (Q_{10}) of 2.3 (Eq. 4). These values are typical for an enzyme-mediated process and exceed those expected for a simple diffusion-mediated process (Van Winkle 1995).

The transport cycle for electrogenic NaPi-II cotransporters is proposed to involved transitions between a number of states (Forster et al. 2002), and the contributions of the respective partial reactions between states to the overall temperature dependence can therefore best be studied using electrophysiology. Figure 2A shows representative current recordings from the same oocytes expressing flounder NaPi-IIb at 20°C and 10°C in response to voltage steps for 80 ms in the range –160 to +80 m*V* from a holding potential of –60 m*V*. At 20°C, in the absence of external P_i (with superfusion in ND100), we observed presteady-state relaxations superimposed on the oocyte capacitive charging transient, as we have previously reported for flounder NaPi-IIb (Forster et al. 1997, 2000; Virkki et al. 2006a, b). These relaxations were suppressed in the presence of 1 mM P_i. At 10°C, the relaxations were clearly slower, and therefore we doubled the pulse width to ensure that a steady-state current was reached. Like the data at 20°C, the relaxations at 10°C were suppressed with 1 mM P_i. The P_i-dependent current was obtained by subtracting the records in ND100 from the corresponding records in ND100+P_i (Fig. 2A, lower data set). The steady-state P_i-dependent current (I_{P_i}) was smaller at the lower temperature. Figure 2B shows pooled *I-V* data (n = 4) obtained from similar records as shown in Figure 2A, normalized to I_{P_i} at –100 m*V* at 20°C, for a larger range of temperatures and intermediate test voltages. For this steady-state analysis, we omitted the responses for $V \geq 0$ m*V* because the data were contaminated by endogenous activating currents.

We have previously reported that the type II Na^+/P_i cotransporters exhibit an uncoupled leak mode (Forster et al. 1998, 2000). This can be observed using the P_i transport blocker PFA, which specifically inhibits the leak current. To determine the temperature dependence of the leak-mode activity, we recorded the response to PFA (1 mM) (*not shown*) at different temperatures and normalized the data to I_{P_i} for each cell in response to 1 mM P_i at –100 m*V* and 20°C. The steady-state PFA-induced changes in holding current (I_{PFA}) for the flounder isoform were typically ≤10% of I_{P_i} (Forster et al. 2000) and, like I_{P_i}, strongly temperature-dependent as shown for the data sets pooled and normalized to the corresponding I_{P_i} for each cell in Figure 2C. Note that each data point is the difference between the holding current in ND100 + PFA and ND100,

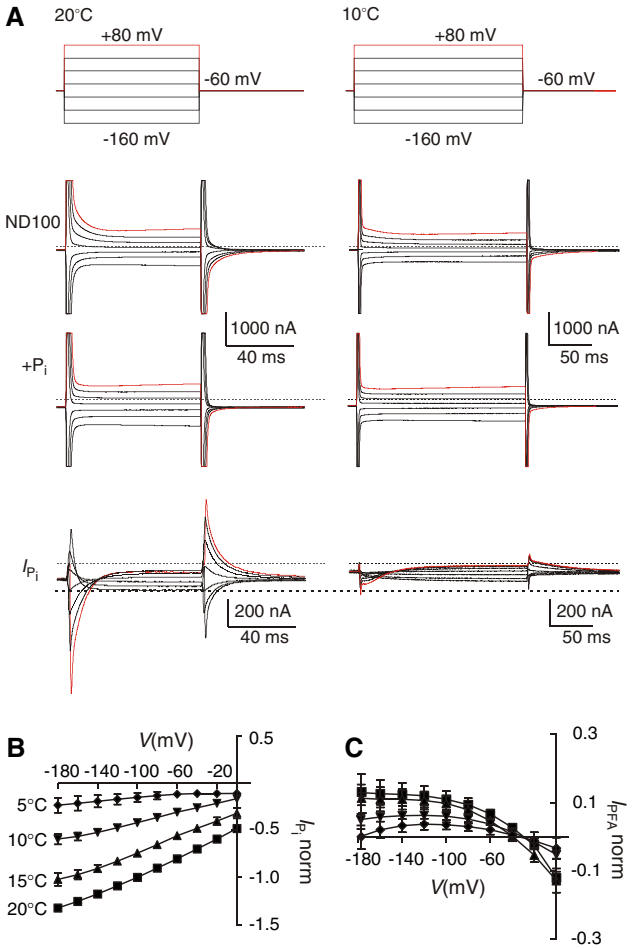

Fig. 2 Steady-state temperature dependence of substrate-induced currents. (*A*) Representative current recordings from an oocyte that expressed NaPi-IIb, made at 20°C (*left*) and 10°C (*right*). Currents were recorded in response to the voltage jump protocol from a holding potential of –60 m*V* to potentials in the range –160 to 80 m*V* at 40-m*V* intervals, in the absence (ND100) and presence of P_i (1 mM, total). *Dotted lines* indicate the steady-state zero current level. The P_i-dependent current (I_{P_i}) was obtained from the difference between corresponding traces in ND100+P_i and ND100. Note that a longer pulse was used at 10°C to ensure that a steady state was reached. For each data set, traces at +80 m*V* are shown in *red. Dashed line* indicates I_{P_i} at –160 m*V*, 20°C to aid comparison. (*B*) *I-V* plots of I_{P_i} at the indicated temperatures. Data are shown as means ± SEM (n = 4), normalized to I_{P_i} at 20°C and –100 m*V*. (*C*) *I-V* plots of the PFA-induced change in holding current current (I_{PFA}). Data were obtained using the same protocols as in *A* except that 1 mM PFA was substituted for 1 mM P_i. For each oocyte, the I_{PFA} data were first normalized to I_{P_i} for each cell at –100 m*V* before pooling. Same symbols as in *B*

and the NaPi-IIb PFA-inhibited leak current would be given by -I_{PFA}, under the assumption that PFA fully blocks the leak current. Unlike I_{P_i}, these currents showed a current reversal in the range –30 to –20 m*V* that appeared to be temperature-independent. Determination of exact reversal potential was not possible because of the relatively small magnitude of I_{PFA} (current magnitudes in the range 10–15

nA at –100 m*V*) and uncertainties regarding the contribution of endogenous PFA response at potential extremes (Forster et al. 2000).

We compared the temperature dependence of the currents corresponding to the cotransport and leak modes by replotting the normalized *I-V* data in the form of Arrhenius plots (Fig. 3). For I_{P_i}, the data were well described by the fit of a linear regression line over a range of potentials from –180 to 0 m*V* (Fig. 3A). For I_{PFA}, the data were less reliable, particularly near the reversal potential. From the slopes of the Arrhenius plots, we obtained estimates of the activation energy for I_{P_i} and I_{PFA}, as shown in Figure 3C (*see* Eq. 3b). The E_a for I_{P_i} showed little variation with membrane potential and was larger than the E_a for I_{PFA} for all potentials. The mean E_a for I_{P_i} of ~15 kcal mol^{-1} corresponds to Q_{10} ~2.5 (Eq. 4), which is typical for values reported in other studies on electrogenic cotransporter membrane proteins (Beckman and Quick 2001; Binda et al. 2002; Wadiche and Kavanaugh 1998); and for I_{PFA}, the E_a corresponded to a Q_{10} ~2.0.

Temperature Dependence of Presteady-State Relaxations

We next investigated the effect of temperature on the presteady-state relaxations to determine if specific transitions might dominate the temperature dependence of the cotransport function. Figure 4A shows representative presteady-state currents for the ON transition from the holding potential to the step potential, recorded from the same oocyte, superfused with ND100 at four temperatures. In each case, we applied baseline correction to remove the steady-state currents. As we reduced the temperature, the relaxations superimposed on the capacitive charging transient became slower and the initial amplitude decreased. There also appeared to be less charge movement for the same voltage change in the hyperpolarizing direction compared with depolarizing steps, which suggested an alteration in the voltage dependence of the charge distribution. The effect of temperature on the presteady-state relaxations was reversible. This was established for representative experiments (n = 3) in which temperature was reduced progressively from 20°C to 5°C and then the test protocol was repeated at 20°C, whereupon the time course and amount of charge were unchanged (*data not shown*).

We quantified these data by fitting the total relaxation with a double exponential function to yield two time constants, the slower of which (τ_s) is shown superimposed on the total current (Fig. 4A). The voltage dependence of the time constants is shown in Figure 4B for ND100 and in the absence of external Na^+ ions (ND0) and for three temperatures (20°C, 15°C and 10°C) (n = 6). Fits to the data at 5°C proved too unreliable because of noise contamination

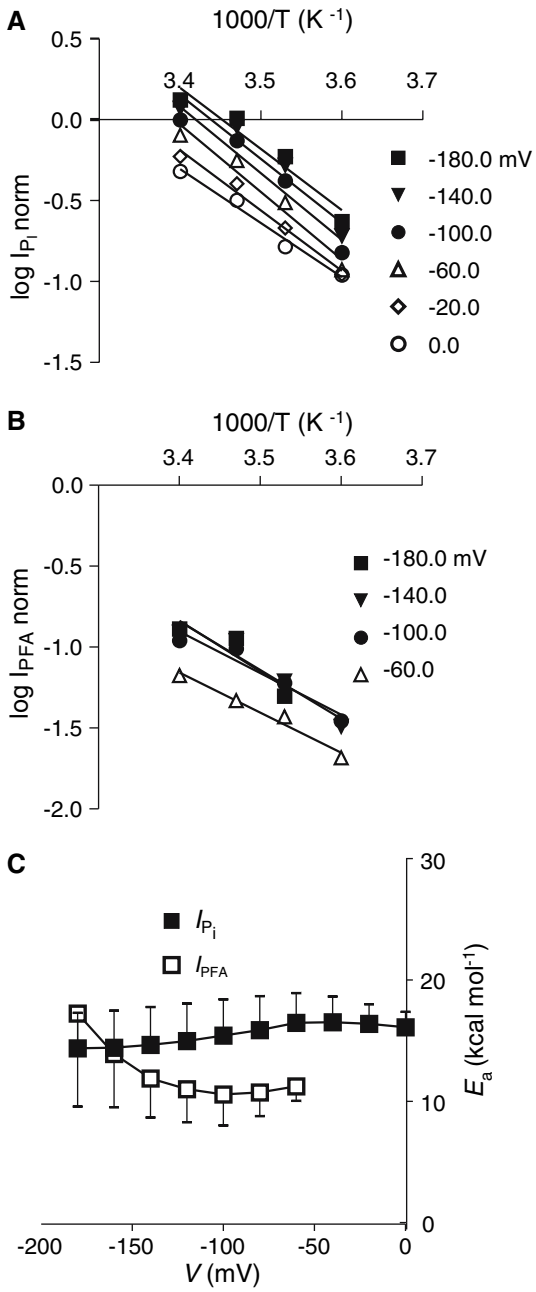

Fig. 3 Temperature dependence of I_{P_i} and I_{PFA}. (*A*) Arrhenius plots of the normalized magnitude of I_{P_i} replotted from the data in Figure 2B for the membrane potentials indicated. *Straight lines* represent linear regression fits to the data points to yield the apparent E_a given by Eq. 3. (*B*) Arrhenius plots for normalized I_{PFA} replotted from the data in Figure 2C for the membrane potentials indicated. *Straight lines* represent linear regression fits to the data points to yield E_a. (*C*) E_a plotted as a function of membrane potential for P_i- (I_{P_i}, *filled squares*) and PFA-induced change in holding current (I_{PFA}, *open squares*). Note that for I_{PFA} we were unable to determine E_a for potentials close to the I_{PFA} reversal potential because of data unreliability

of the signal at low amplitudes. The faster time constant (τ_f) (Fig. 4B, inset) became slower with decreasing temperature and showed little voltage dependence. As in

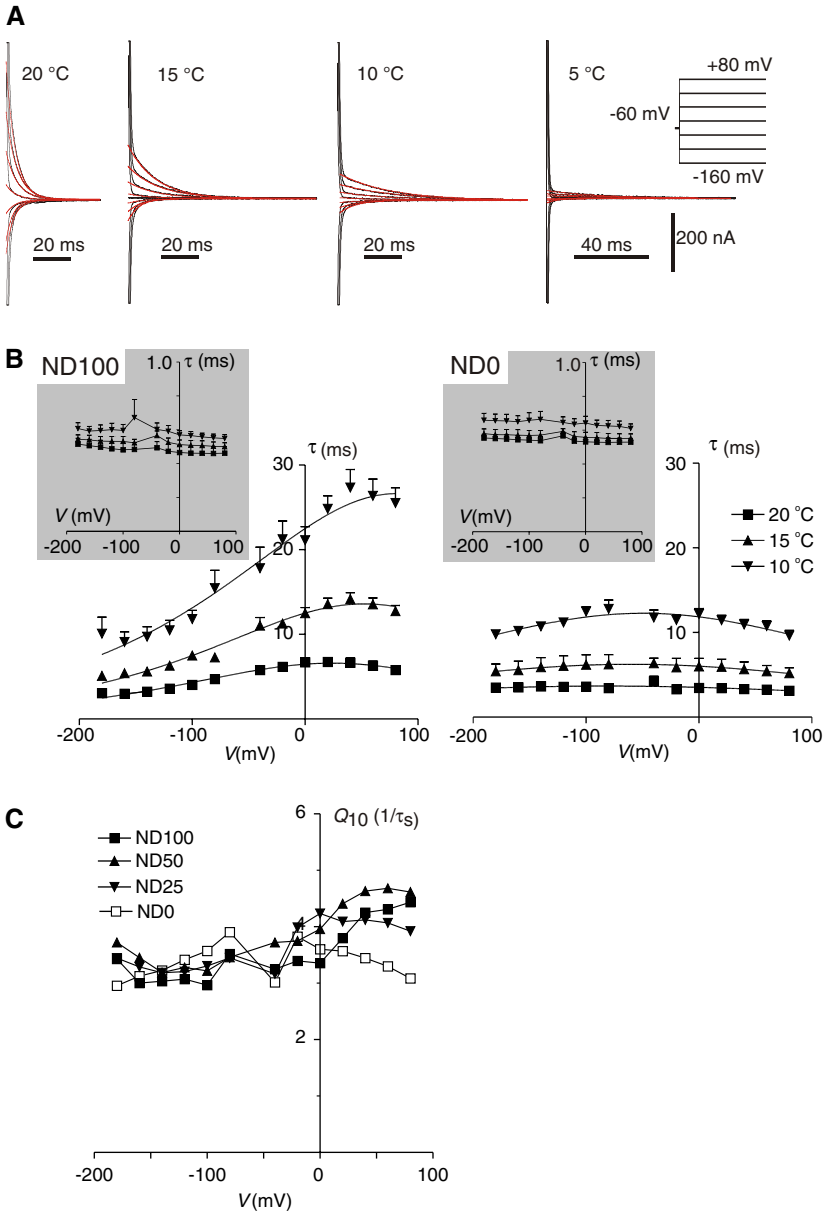

Fig. 4 Temperature effects on the kinetics of presteady-state currents. (*A*) Presteady-state relaxations recorded from the same oocyte in response to voltage steps from a holding potential of –60 m*V* to voltages in the range –180 to +80 m*V* at the four temperatures indicated. The steady-state holding currents were subtracted for each data set. *Red traces* indicate the slower fitted component derived from the two-exponential fit to the complete trace, commencing approximately 1 ms after the voltage step onset. (*B*) Voltage dependence of the main relaxation time constant (τ-*V*) reported by a two-exponential fit to the data in *A* for the three temperatures indicated, corresponding to the fitted curves in *A*. *Continuous lines* are fits with Eq. 2 to the data points. *Left*: Superfusion in ND100. *Right:* Superfusion in ND0. *Inset:* Temperature and voltage dependence of the fast component. Data at 5°C were too unreliable to determine the slow relaxation time constant. (*C*) Voltage dependence of Q_{10} of the reciprocal of the main relaxation time constant ($1/\tau_s$) for the external indicated Na^+ concentrations. Data points are joined by lines for visualization. Q_{10} was calculated from the ratio of $1/\tau_s$ at 20°C to $1/\tau_s$ at 10°C ($n = 6$)

previous studies, we assumed that this component represented the capacitive charging of the oocyte. Its temperature dependence may result from a temperature dependence of the membrane capacitance (White 1970) that would result in slower membrane charging. The small voltage dependence of this component most likely results from a systematic error in the fits because it was observed at all Na^+ concentrations and temperatures.

The slower time constant (τ_s) that we assumed to be associated with NaPi-IIb showed strong temperature and voltage dependence (Fig. 4B, C). For ND100 and ND0 superfusion, τ_s increased approximately threefold for a decrease in temperature from 20°C to 10°C. For ND100 superfusion, the voltage at which τ_s peaked shifted toward depolarizing potentials as the temperature decreased, whereas for ND0, a shift of the peak τ_s was less obvious. When expressed as Q_{10} (Fig. 4C), the temperature dependence of the relaxation rate constant ($1/\tau_s$) showed little dependence on Na^+ for $V < 0$. In contrast, for depolarizing potentials, Q_{10} increased for nonzero Na^+ concentrations. This behavior suggested that, in addition to the overall slowing of the relaxation rates with decreasing temperature, the voltage dependence of the Na^+ interaction with the NaPi-IIb protein was more temperature-dependent than that of the empty carrier alone.

To study the underlying mechanism in more detail, we determined the dependence of charge movement on external Na^+ ranging from 0 (ND0) to 125 (ND125) mM. Numerical integration of the slower relaxations yielded an estimate of the charge (Q_{ON}) moved for each voltage step from V_h to the

corresponding target potential as shown in Figure 5A at two temperatures. To facilitate comparison of data sets, the data were fit with Eq. 1, shifted by the predicted Q_{hyp} and normalized to Q_{max} for ND100 at 20°C. At 20°C (Fig. 5A, left), a decrease in external Na^+ resulted in a hyperpolarizing shift in the charge distribution similar to the shift reported in previous studies (Forster et al. 1997; Virkki et al. 2006a, b). At 10°C, a similar hyperpolarizing shift with decreasing Na^+ concentration was documented. For a given Na^+ concentration, there was also a relative hyperpolarizing shift of the charge distribution at the lower temperature. For superfusion in ND100, the Q-V behavior with respect to temperature corresponded qualitatively to that observed for the peak of the τ_s-V at ND100 (Fig. 4B, left).

The temperature dependence of the Boltzmann fit parameters with varying external Na^+ is summarized in

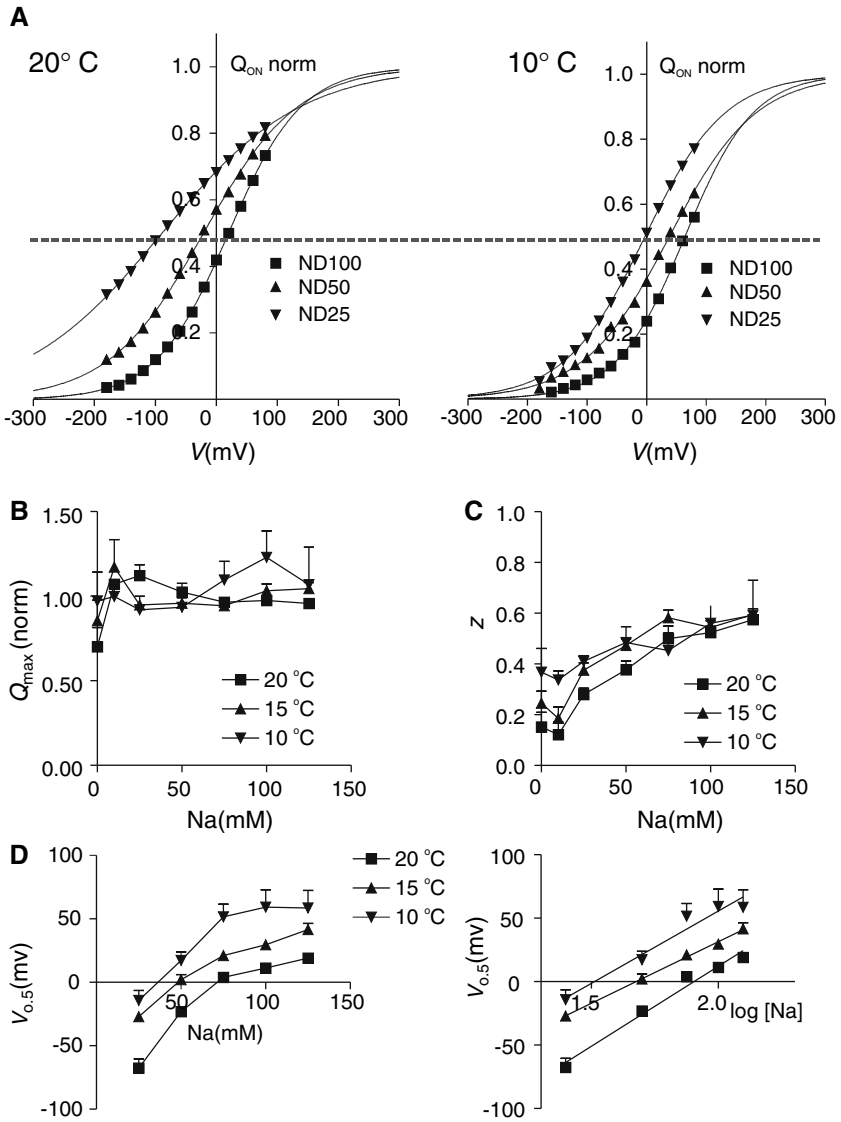

Fig. 5 Temperature dependence of fit parameters from Q-V data. (*A*) Voltage dependence of the charge (Q-V) associated with the slow relaxation component for the same cell as in Fig. 4A *A* at 20°C (*left*) and 10°C (*right*) at three external Na^+ concentrations (ND100, 100 mM; ND50, 50 mM; ND25, 25 mM). *Continuous lines* are fits with Eq. 1 to the data points. Data for each Na^+ concentration were normalized to the predicted Q_{max} from the curve fit and offset by Q_{hyp}. The fit parameters were as follows: at 20°C, $V_{0.5}$ = 20 ± 2 m*V* (ND100), –21 ± 4 m*V* (ND50), –90 ± 9 m*V* (ND25) and z = 0.42 ± 0.01 (ND100), 0.32 ± 0.02 (ND50), 0.22 ± 0.02 (ND25); at 10°C, $V_{0.5}$ = 65 ± 17 m*V* (ND100), 38 ± 19 m*V* (ND50), –2.8 ± 4.2 m*V* (ND25) and z = 0.44 ± 0.05 (ND100), 0.35 ± 0.05 (ND50), 0.37 ± 0.02 (ND25). The absolute Q_{max} values for individual cells at 20°C and 100 mM Na^+ ranged 11.5–29.6 nC. (*B*) Maximum available charge, Q_{max}, reported by Boltzmann fit plotted as a function of Na^+ pooled from six cells and normalized to the Q_{max} reported from fit to ND100 data at 20°C. (*C*) Apparent valence, z, reported by Boltzmann fit plotted as a function of Na^+ (n = 6). (*D*) Midpoint voltage ($V_{0.5}$) reported by Boltzmann fit plotted as a function of Na^+ (n = 6) and the same data replotted on a log[Na] scale and fitted with a linear regression line with slopes 126 ± 11 m*V* (20°C), 97 ± 3 m*V* (15°C) and 114 ± 15 m*V* (10°C)

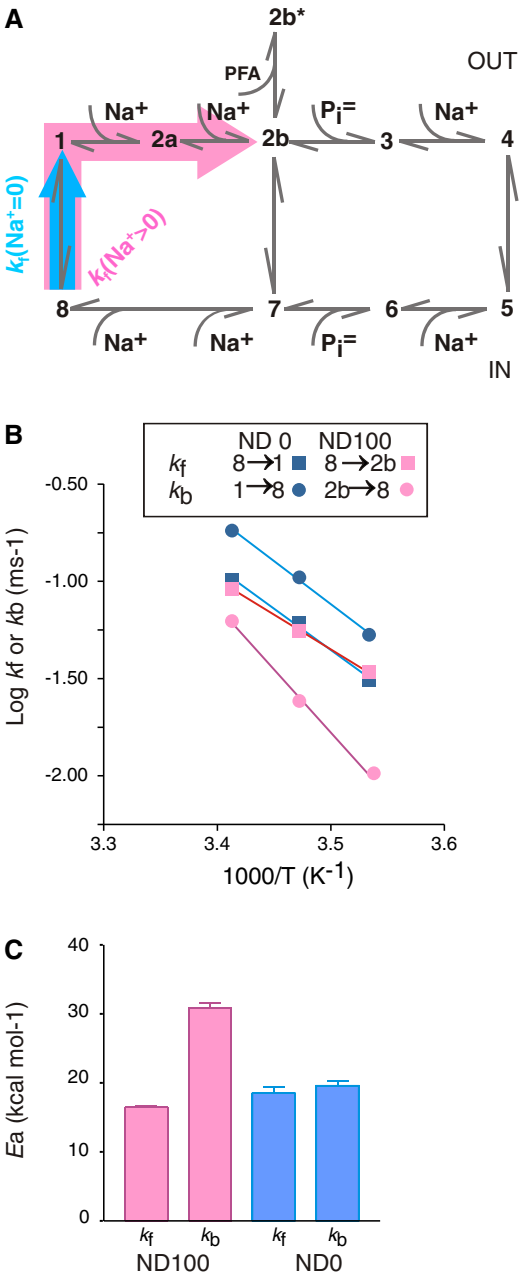

Fig. 6 Temperature dependence of partial reaction rates. (*A*) A kinetic scheme of electrogenic type II Na^+/P_i cotransport. Two Na^+ ions are proposed to bind before P_i binding can occur, and transition 2a⇒2b is voltage-dependent (Virkki et al. 2006b). The PFA-blockable leak current is, in part, due to the translocation of Na^+ ions between states 2a or 2b and 7. In the presence of PFA, the transporter occupies an inactive state (2b*). With saturating P_i, the transport cycle proceeds through states 3 and 4 to the fully loaded carrier. *Pink block arrow* indicates the partial reactions that contribute to presteady-state charge movement with Na^+ in the superfusion medium. *Blue block arrow* indicates the empty carrier partial reaction (ND0 superfusion). The direction of the forward reaction (k_f) is indicated for each. (*B*) Arrhenius plots of the zero-voltage rate constants (k_f, k_b) derived from fitting the time constants of the presteady-state relaxations (Fig. 4B) to Eq. 2. *Inset* identifies the rate constant with the lumped transitions according to the kinetic scheme in *A* for the two experimental superfusion conditions: ND100 (*pink symbols*) and ND0 (*blue symbols*). For ND100 superfusion, three partial reactions are lumped into one. Lines are linear regression fits to data points. (*C*) E_a for k_f and k_b derived from the slopes of the linear regression fits to the data in *B*. Error bars indicate error reported by fit

Figure 5B-D (n = 6). As expected, Q_{max}, the total mobile charge, normalized to that at ND100 and 20°C for each cell (to account for differences in expression level) was relatively insensitive to temperature (Fig. 5B). At 10°C, this parameter was subject to more uncertainty, where the signal-to-noise ratio was worse. Moreover, the normalized Q_{max} remained reasonably constant for nonzero Na^+. The apparent valence (z), derived from the maximum slope of the Boltzmann fits, decreased with decreasing Na^+; however, there was no statistical significance with respect to temperature (one-way analysis of variance, $P < 0.05$) (Fig. 5C). Finally, the voltage at which 50% of the charge was moved ($V_{0.5}$) decreased with diminishing Na^+ (Fig. 5D), and there was a clear temperature-dependent shift of this parameter. When the $V_{0.5}$ data were replotted on a log [Na^+] scale, the linear regression fits gave slopes for Na^+ varying from 125 to 25 mM of 126 ± 11 mV (20°C), 97 ± 3 mV (15°C) and 114 ± 15 mV (10°C). These slopes were not significantly different over the 10°C range of temperature ($P < 0.05$).

Discussion

This report describes the effect of temperature on the kinetics of a type II Na^+/P_i cotransporter expressed in *Xenopus* oocytes. Our estimates of the temperature dependence for the cotransport mode behavior obtained from uptake and electrophysiology assays, expressed as E_a, are in good agreement with one another. This is to be expected because we have shown that there is a tight correlation between charge translocation and P_i cotransport (Forster et al. 1999; Virkki et al. 2005b). Moreover, the corresponding Q_{10} of ~2.3–2.5 for the P_i-dependent current agrees with estimates reported for other cation-coupled electrogenic cotransporters, such as SGLT1 (Hazama et al. 1997; Parent and Wright 1993), rGAT1 (Binda et al. 2002) and GAT4 (Karakossian et al. 2005). For the cotransport mode of NaPi-IIb, the E_a of the P_i-dependent current (I_{Pi}) was essentially independent of membrane potential in the range where the transport rate is strongly voltage-dependent, i.e., for $V < 0$ mV. If we assume that 1 mM P_i is sufficient to ensure ''V_{max}'' conditions for all temperatures investigated, then our finding also accords with the behavior of SGLT1, for which the temperature dependence of the predicted maximum electrogenic sugar-induced

current was also reported to be independent of V (Parent and Wright 1993). A V_{max} effect on the electrogenic activity of the human NaPi-IIa isoform expressed in *Xenopus* oocytes was also documented, with a Q_{10} of ~3 (Wagner 1998), and this study also established that the apparent affinity of P_i was not significantly altered by temperature.

For the leak mode, quantified as I_{PFA}, E_a was smaller than that for the cotransport mode. The uncertainty in the fit, especially for hyperpolarizing potentials, did not allow us to make a definite statement about the voltage dependence of E_a for the leak mode. The difference in E_a for these two modes suggests distinct transport mechanisms. Certainly, compared to two other cotransport systems, the temperature dependence of the NaPi-IIb leak mode is too large for it to result only from a simple channel-like conductance. For the glutamate transporter EAAT1 (Beckman and Quick 2001; Wadiche and Kavanaugh 1998) and the GABA transporter GAT4 (Karakossian et al. 2005), Q_{10} values close to unity were found for their respective leak modes, consistent with an electrodiffusive mechanism. In contrast, for the sodium-coupled glucose transporter SGLT1, an $E_a = 21 \pm 3$ kcal mol^{-1} was documented (Loo et al. 1999). Like NaPi-IIb in the present study, this finding suggests that the leak mode in SGLT1 also involves large conformational changes. On the other hand, from the steady-state data alone, we are unable to exclude the possibility that there is an additional ''channel'' component of the leak pathway, which may also be PFA-sensitive and conductive for other ions, including Cl^- (I. C. Forster, L. V. Virkki, A. Bacconi, unpublished observations). Caution should also be observed with respect to overinterpreting the apparent differences in E_a for the two modes, given the uncertainties reported by the fitting algorithm and the fact that for flounder NaPi-IIb I_{PFA} is typically ≤10% of I_{Pi} and therefore more prone to contamination from endogenous PFA-dependent currents (Forster et al. 2000). It should also be noted that E_a determined from the Arrhenius plot represents an effective estimate in which the transport process (leak or cotransport mode) is lumped into a single reaction that obeys first-order kinetics. This is an oversimplification because a number of partial reactions have already been identified as contributors to the overall cotransport cycle (Forster et al. 1998; Virkki et al. 2005b, 2006b), any of which might dominate the overall temperature dependence (Fig. 6A). From our data, we can conservatively conclude that the estimates of E_a for the leak mode strongly indicate that conformational changes take place that are inconsistent with an exclusively electrodiffusive transport process.

From the presteady-state data analysis, we found that the relaxations in the presence and absence of external Na^+ showed significant temperature dependence (Fig. 4). As expected, the predicted Q_{max} from the Boltzmann data was insensitive to temperature for Na^+ >25 mM. This result confirmed that we were able to detect all the charge over the temperature range used, except at low Na^+ concentrations, where the curve fitting and numerical integration were less reliable. It also confirmed that the number of active transporters in the membrane did not change with temperature. Moreover, we observed no significant temperature dependence of the apparent valence (z) for the Boltzmann fit.[1] In contrast, the midpoint voltage ($V_{0.5}$) of the Q-V distribution for a given Na^+ concentration was shifted toward depolarizing potentials as the temperature was lowered (Fig. 5C), whereas the slopes of the $V_{0.5}$ *vs.* log[Na^+] plots were not statistically altered by temperature. The linear dependence of $V_{0.5}$ on log[Na^+] is the behavior predicted, e.g., for a two-state ''ion-well'' model for voltage–dependent Na^+ interaction with a carrier (Mager, Cao and Lester 1998; Mager et al. 1996; Virkki et al. 2006b). The Q-V relation for this model is a modified version of Eq. 1 to take account of Na^+ dependence of the binding reaction:

$$Q = Q_{max}/[(1 + \{[Na^+]/K^{Na}\exp(-Ve\delta/kT)\}n_{Na}] + Q_{hyp} \quad (5)$$

where K^{Na} is a zero-voltage Na^+ binding constant that corresponds to [Na^+] when half the charge has moved and n_{Na} is the number of Na^+ ions that bind at a hypothetical site located a fraction δ through the membrane field.[2] For NaPi-IIb, we have shown that $n_{Na} = 1$ (Virkki et al. 2006b) and the slope of $V_{0.5}$ *vs.* log[Na^+] = 2.303 kT/(eδ), from which we can estimate δ. Our data (Fig. 5C) suggest that δ is not a function of temperature, which implies that Na^+ ions move through the same fraction of the transmembrane field, independent of temperature. The mean of the slopes at the three test temperatures gave $\delta = 0.51$, which is consistent with our previous analyses of the NaPi-IIb presteady-state kinetics (Virkki et al. 2006a, b). On the other hand, the intercept with the log[Na^+] axis shifted to the left with decreasing temperature, which indicated that K^{Na} decreased with decreasing temperature. In terms of the simple two-state model for charge translocation (see Materials and Methods), K^{Na} can also be expressed as the ratio of the zero-voltage rates (k_f, k_b), and therefore the observed dependence of K^{Na} on temperature could result from a change in either rate constant or both.

[1] The dependence of z on [Na^+] is a consequence of fitting a single Boltzmann function to the Q-V data. The valence estimated from the single fit is a weighted value that depends on the relative contributions from the empty carrier and Na^+ binding partial reactions. Similar behavior was observed by fitting a single Boltzmann to presteady-state data generated by a three-state model that simulates the empty carrier and one voltage-dependent Na^+ binding step (I. C. Forster, unpublished data).

Table 1 Temperature dependence of fit parameters for τ-V data

Temp (°C)	ND100			ND0		
	k_f (ms^{-1})	k_b (ms^{-1})	z	k_f (ms^{-1})	k_b (ms^{-1})	z
20	0.092 ± 0.004	0.063 ± 0.003	0.40 ± 0.02	0.102 ± 0.009	0.183 ± 0.011	0.18 ± 0.05
15	0.056 ± 0.003	0.024 ± 0.003	0.40 ± 0.03	0.061 ± 0.001	0.105 ± 0.002	0.23 ± 0.01
10	0.034 ± 0.002	0.010 ± 0.002	0.37 ± 0.04	0.031 ± 0.001	0.053 ± 0.002	0.27 ± 0.02

Fit parameters are given by Eq. 3. Errors are standard errors reported by fit algorithm

To distinguish between these possibilities, we fitted the τ_s-V data (Fig. 4B) for superfusion in ND100 with Eq. 2 to obtain estimates for k_f and k_b, as summarized in Table 1. These data confirmed that both rates became slower with decreasing[2] temperature. To further quantify the temperature dependence of the fit-derived reaction rates, we plotted these data in the Arrhenius form (Fig. 6B). For ND100 superfusion, the data show that the temperature dependence of the effective backward rate (k_b) of the lumped Na^+ interaction (i.e., by considering the transitions 8⇔1⇔2a⇔2b as a single transition [Fig. 6A]) was greater than that of the effective forward reaction (k_f). In terms of a simple ion–well model, we interpret this as indicating that the apparent affinity for Na^+ ions increases with decreasing temperature. We also fitted the τ_s-V data for ND0 superfusion with Eq. 2, to investigate the temperature dependence of the empty carrier (transition 8⇔1, Fig. 6A). Here, the Arrhenius analysis showed that the temperature dependence for the effective k_b and k_f was similar and close to that of k_f with ND100 superfusion (Fig. 6B). Figure 6C summarizes these findings in terms of the activation energy for each rate constant.

Our finding that E_a determined under voltage clamp for the cotransport mode is essentially independent of membrane potential suggests that a major electroneutral conformational change occurs during the transport cycle. One likely candidate for the corresponding transition, according to the scheme of Figure 6A, is the translocation of the fully loaded carrier (transition 4⇔5), which we have previously proposed to be electroneutral (Forster et al. 1998) but without experimental evidence. In the present study, this proposal is supported by our finding that E_a for the empty carrier zero-voltage rate constants corresponds closely to the E_a estimated from the steady-state analysis for the cotransport mode. Thus, in the absence of membrane potential, the partial reactions that describe the reorientation of the empty and fully loaded carrier are energetically similar. On the other hand, given that we have no information about the voltage dependence of the partial reactions between intracellularly oriented states, we cannot exclude that conformational changes associated with other transitions between states 5 and 8 also contribute to the voltage-independent activation energy observed for cotransport.

[2] In applying this model to NaPi-IIb, we have lumped the empty carrier transition (1–8, Fig. 6A) and Na^+ binding transitions (1–2a, 2a–2b) into a single transition. A more accurate description of the presteady-state kinetics would require fitting the presteady-state relaxations to >2 exponentials and using at least a two Boltzmann fit to the data. We were unable to extract more than one component of nonendogenous presteady-state charge movement by exponential curve fitting with confidence. Moreover, attempts to fit a double Boltzmann function to our Q-V data (e.g., as undertaken by Krofchick, Huntley and Silverman [2004] for SGLT1) were equally unsuccessful because of fit uncertainties with the larger number of free parameters.

Acknowledgement This work was supported by grants to H. M. from the Swiss National Science Foundation and the Gebert Rüf Foundation (http://www.grstiftung.ch).

References

Accardi A, Miller C (2004) Secondary active transport mediated by a prokaryotic homologue of ClC Cl^- channels. Nature 427:803–807

Adams SV, DeFelice LJ (2002) Flux coupling in the human serotonin transporter. Biophys J 83:3268–3282

Beckman ML, Quick MW (2001) Substrates and temperature differentiate ion flux from serotonin flux in a serotonin transporter. Neuropharmacology 40:526–535

Binda F, Bossi E, Giovannardi S, Forlani G, Peres A (2002) Temperature effects on the presteady-state and transport-associated currents of GABA cotransporter rGAT1. FEBS Lett 512:303–307

Birnir B, Loo DD, Wright EM (1991) Voltage-clamp studies of the Na^+/glucose cotransporter cloned from rabbit small intestine. Pfluegers Arch 418:79–85

Chen XZ, Coady MJ, Jalal F, Wallendorff B, Lapointe JY (1997) Sodium leak pathway and substrate binding order in the Na^+-glucose cotransporter. Biophys J 73:2503–2510

DeFelice LJ (2004) Transporter structure and mechanism. Trends Neurosci 27:352–359

Eskandari S, Loo DD, Dai G, Levy O, Wright EM, Carrasco N (1997) Thyroid Na^+/I^- symporter. Mechanism, stoichiometry, and specificity. J Biol Chem 272:27230–27238

Forster I, Hernando N, Biber J, Murer H (1998) The voltage dependence of a cloned mammalian renal type II Na^+/P_i cotransporter (NaPi-2). J Gen Physiol 112:1–18

Forster IC, Biber J, Murer H (2000) Proton-sensitive transitions of renal type II Na^+-coupled phosphate cotransporter kinetics. Biophys J 79:215–230

Forster IC, Kohler K, Biber J, Murer H (2002) Forging the link between structure and function of electrogenic cotransporters:

The renal type IIa Na^+/P_i cotransporter as a case study. Prog Biophys Mol Biol 80:69–108

Forster IC, Loo DD, Eskandari S (1999) Stoichiometry and Na^+ binding cooperativity of rat and flounder renal type II Na^+-P_i cotransporters. Am J Physiol 276:F644-F649

Forster IC, Wagner CA, Busch AE, Lang F, Biber J, Hernando N, Murer H, Werner A (1997) Electrophysiological characterization of the flounder type II Na^+/P_i cotransporter (NaPi-5) expressed in *Xenopus laevis* oocytes. J Membr Biol 160:9–25

Hazama A, Loo DD, Wright EM (1997) Presteady-state currents of the rabbit Na^+/glucose cotransporter (SGLT1). J Membr Biol 155:175–186

Karakossian MH, Spencer SR, Gomez AQ, Padilla OR, Sacher A, Loo DD, Nelson N, Eskandari S (2005) Novel properties of a mouse gamma-aminobutyric acid transporter (GAT4). J Membr Biol 203:65–82

Kohler K, Forster IC, Stange G, Biber J, Murer H (2002a) Identification of functionally important sites in the first intracellular loop of the NaPi-IIa cotransporter. Am J Physiol 282:F687–F696

Kohler K, Forster IC, Stange G, Biber J, Murer H (2002b) Transport function of the renal type IIa Na^+/P_i cotransporter is codetermined by residues in two opposing linker regions. J Gen Physiol 120:693–703

Krofchick D, Huntley SA, Silverman M (2004) Transition states of the high-affinity rabbit Na^+/glucose cotransporter SGLT1 as determined from measurement and analysis of voltage-dependent charge movements. Am J Physiol 287:C46–C54

Loo DDF, Hirayama BA, Meinild A-K, Chandy G, Zeuthen T, Wright EM (1999) Passive water and ion transport by cotransporters. J Physiol 518:195–202

Mager S, Cao Y, Lester HA (1998) Measurement of transient currents from neurotransmitter transporters expressed in *Xenopus* oocytes. Methods Enzymol 296:551–566

Mager S, Kleinberger-Doron N, Keshet GI, Davidson N, Kanner BI, Lester HA (1996) Ion binding and permeation at the GABA transporter GAT1. J Neurosci 16:5405–5414

Otis TS, Jahr CE (1998) Anion currents and predicted glutamate flux through a neuronal glutamate transporter. J Neurosci 18:7099–7110

Parent L, Wright EM (1993) Electrophysiology of the Na^+/glucose cotransporter. Soc Gen Physiol Ser 48:263–281

Segel IH (1976) Biochemical Calculations. Wiley, New York

Sonders MS, Amara SG. (1996) Channels in transporters. Curr Opin Neurobiol 6:294–302

Van Winkle L (1995) Biomembrane Transport. Academic Press, San Diego

Virkki LV, Forster IC, Bacconi A, Biber J, Murer H (2005a) Functionally important residues in the predicted 3rd transmembrane domain of the type IIa sodium-phosphate co-transporter (NaPi-IIa). J Membr Biol 206:227–238

Virkki LV, Forster IC, Biber J, Murer H (2005b) Substrate interactions in the human type IIa sodium-phosphate cotransporter (NaPi-IIa). Am J Physiol 288:F969–F981

Virkki LV, Forster IC, Hernando N, Biber J, Murer H (2003) Functional characterization of two naturally occurring mutations in the human sodium-phosphate cotransporter type IIa. J Bone Miner Res 18:2135–2141

Virkki LV, Murer H, Forster IC (2006a) Mapping conformational changes of a type IIb Na^+/P_i cotransporter by voltage clamp fluorometry. J Biol Chem 281:28837–28849

Virkki LV, Murer H, Forster IC (2006b) Voltage clamp fluorometric measurements on a type II Na^+-coupled P_i cotransporter: Shedding light on substrate binding order. J Gen Physiol 127:539–555

Wadiche JI, Kavanaugh MP (1998) Macroscopic and microscopic properties of a cloned glutamate transporter/chloride channel. J Neurosci 18:7650–7661

Wagner CA (1998) Elektrophysiologische Untersuchungen an den renalen Natrium-Phosphat-Kotransportern NaPi-3 (Mensch) und NaPi-7 (Maus). Doctoral diss., University of Tübingen, Tübingen

White SH (1970) A study of lipid bilayer membrane stability using precise measurements of specific capacitance. Biophys J 10:1127–1148

Yao X, Pajor AM (2000) The transport properties of the human renal Na(+)-dicarboxylate cotransporter under voltage-clamp conditions. Am J Physiol 279:F54–F64